

# Quantitative multi-slice computed tomography assessment of the mitral valvular complex for transcatheter mitral valve interventions part 2: geometrical measurements in patients with functional mitral regurgitation



Pascal Thériault-Lauzier<sup>1</sup>, PhD; Magdalena Dorfmeister<sup>2</sup>, MD; Darren Mylotte<sup>1</sup>, MD; Ali Andalib<sup>1</sup>, MD; Marco Spaziano<sup>1</sup>, MD; Philipp Blanke<sup>3</sup>, MD; Giuseppe Martucci<sup>1</sup>, MD; Rüdiger Lange<sup>2</sup>, MD, PhD; Jonathon Leipsic<sup>3</sup>, MD; Luc Bilodeau<sup>1</sup>, MD; Nicolo Piazza<sup>1,2\*</sup>, MD, PhD

1. Department of Medicine, Division of Cardiology, McGill University Health Centre, Montreal, Quebec, Canada; 2. Department of Cardiovascular Surgery, German Heart Centre Munich, Munich, Germany; 3. Department of Radiology, University of British Columbia, Vancouver, Canada

## KEYWORDS

- mitral regurgitation
- mitral valve
- multi-slice computed tomography
- transcatheter heart valve
- transcatheter mitral valve replacement

## Abstract

**Aims:** Transcatheter mitral valve replacement (TMVR) is an emerging technology with the potential to treat patients with mitral regurgitation at excessive risk for mitral valve surgery. Geometrical measurements of the mitral valvular complex may have implications for the design of TMVR devices and for patient selection. This study sought to quantify the dynamic geometry of the mitral valvular complex in patients with significant functional mitral regurgitation (FMR) using multi-slice computed tomography (MSCT).

**Methods and results:** MSCT images were acquired in 32 patients with symptomatic, significant FMR. Two independent observers analysed image sets using a dedicated software package and a standard measurement methodology. In patients with FMR, the mean mitral annulus intercommissural and aorto-mural diameters were, respectively, 41.5±5.2 mm and 38.7±5.9 mm in systole, and were 41.5±4.4 mm and 40.0±4.7 mm in diastole. In patients without MR, the diameters were, respectively, 33.6±5.1 mm and 28.8±8.0 mm in systole, and 36.2±4.5 mm and 31.6±7.9 mm in diastole. The obstacle-free zone below the mitral annulus averaged more than 20.0 mm and varied by less than 1 mm between systole and diastole, which is not statistically significant. The aorto-mitral angle was 129.7±10.5° in systole and 131.0±9.4° in diastole.

**Conclusions:** The mitral annulus is larger in dimension, more circular, and less dynamic in patients with FMR. The obstacle-free zone below the mitral annulus is relatively constant during the cardiac cycle. Measurements of the mitral valvular apparatus vary considerably between patients, which suggests that tri-dimensional imaging will play an important role in the sizing of TMVR devices.

\*Corresponding author: McGill University Health Centre, Department of Medicine, Division of Interventional Cardiology, 687 Pine Avenue West, Montreal, Quebec, H3A 2B4, Canada. E-mail: nicolopiazza@mac.com

## Abbreviations

|             |                                        |
|-------------|----------------------------------------|
| <b>LVOT</b> | left ventricular outflow tract         |
| <b>MPR</b>  | multi-planar reconstruction            |
| <b>MSCT</b> | multi-slice computed tomography        |
| <b>TAVR</b> | transcatheter aortic valve replacement |
| <b>TMVR</b> | transcatheter mitral valve replacement |

## Introduction

Mitral regurgitation (MR) is the most prevalent valvular heart disease in adults<sup>1</sup>. Unfortunately, due to advanced disease or comorbidities, patients are often never operated surgically. To fill this therapeutic gap, and bolstered by the success of transcatheter aortic valve implantation (TAVI)<sup>2</sup>, a substantial effort has been directed towards the development of transcatheter mitral valve implantation. A handful of patients have recently been treated with experimental transcatheter mitral valves in Denmark (2012), Canada (2014), and the United Kingdom (2014).

The mitral valvular complex includes the mitral annulus, mitral leaflets, papillary muscles, the left ventricle and the left atrium<sup>3</sup>. The complex may also interact with the left ventricular outflow tract (LVOT). These structures undergo several geometrical modifications in patients with MR<sup>4</sup>. Some of these changes, regardless of their contribution to the pathogenesis of MR, may be critical in the context of transcatheter mitral valve therapies.

The high spatial and temporal resolution of multi-slice computed tomography (MSCT) makes this imaging modality an ideal tool to study the geometry of the mitral valvular complex. Herein, we apply a systematic MSCT measurement methodology specifically designed for transcatheter mitral valve therapies<sup>5</sup> to characterise the mitral valvular complex in patients with functional MR (FMR). To draw a comparison with our measurements, we also performed a meta-analysis of studies reporting measurements of the mitral valvular complex in patients without MR. The information gathered in this study may be valuable in determining patient selection criteria for transcatheter mitral valve therapies. This study may also provide important data for the design of transcatheter mitral valve devices.

## Methods

### STUDY POPULATION

In this article series, the patients studied were recruited from the PTOLEMY-2 (NCT00787293) and PTOLEMY2Canada (NCT00815386) clinical trials of the Viacor percutaneous transvenous mitral annuloplasty system (Viacor, Inc., Wilmington, MA, USA) from 15 European and Canadian centres. Written consent was obtained from patients and the trials were conducted with the approval of institutional ethics review boards. The trials were conducted to evaluate the implantation of this device in patients in heart failure with functional MR. The PTOLEMY-2 and PTOLEMY2Canada studies were suspended due to a high rate of complications. At the conclusion of studies, MSCT data sets were made available for research purposes to collaborating investigators, including authors of this manuscript. Preoperative MSCT images

were available in 32 patients: 15 scans included only a diastolic phase and 17 scans included both a systolic and a diastolic phase.

### DATA ACQUISITION

MSCT scanners from three manufacturers – GE Healthcare (Waukesha, WI, USA) in four patients, Siemens Healthcare (Erlangen, Germany) in 26 patients, and Philips Healthcare (Eindhoven, The Netherlands) in two patients – were used in this study. The scanning protocol varied between each of the centres involved in the PTOLEMY-2 and PTOLEMY2Canada trials but overall it fulfilled the guidelines described in part 1 of this article. Electrocardiographic gating was used in all patients. Diastolic phases were available in 32 patients, with a mean R-R phase of 75.4%. Of these patients, 17 had also been scanned in systole, with a mean R-R phase of 38.5%. Iodinated contrast agent was injected in all patients.

As a part of trial protocols, patients were evaluated using echocardiography. Echocardiographic data were gathered at each centre and were sent to Duke Clinical Research Institute core laboratory, Durham, NC, USA, for centralised analysis. Left ventricular ejection fraction presented in **Table 1** was estimated using Simpson's biplane method of discs.

### MSCT IMAGE ANALYSIS

Two trained and independent observers performed the MSCT image analysis on the 32-subject data set using 3mensio Structural Heart 6.1 (Pie Medical Imaging BV, Maastricht, The Netherlands). This software package offers a dedicated workflow for assessment of the mitral valve<sup>6</sup>. It also incorporates measurement tools for tri-dimensional distances, angles, and regions of interest.

### MITRAL VALVULAR COMPLEX GEOMETRY

The measurements performed in this study can be classified based on anatomical structures. We highlight salient points of the systematic measurement methodology in this section.

**Table 1. Baseline characteristics of study population.**

|                                        |                      |           |
|----------------------------------------|----------------------|-----------|
| Subjects, n                            |                      | 32        |
| Age*, years                            |                      | 70.1±11.7 |
| Female gender, n (%)                   |                      | 13 (40.6) |
| Body surface area*, m <sup>2</sup>     |                      | 1.85±0.20 |
| Left ventricular ejection fraction*, % |                      | 34.8±11.4 |
| MR severity                            | Mild, n (%)          | 2 (6.3)   |
|                                        | Moderate, n (%)      | 15 (46.9) |
|                                        | Severe, n (%)        | 15 (46.9) |
| MR aetiology                           | Ischaemic, n (%)     | 15 (46.9) |
|                                        | Non-ischaemic, n (%) | 9 (28.1)  |
|                                        | Not reported, n (%)  | 8 (25.0)  |
| NYHA functional class                  | I, n (%)             | 0 (0.0)   |
|                                        | II, n (%)            | 5 (15.6)  |
|                                        | III, n (%)           | 22 (68.8) |
|                                        | IV, n (%)            | 2 (6.3)   |
|                                        | Not reported, n (%)  | 3 (9.4)   |

\* mean±standard deviation.

The mitral annulus was selected using a tridimensional spline with 16 control points. The intercommissural diameter was measured along the line segment that is parallel to the opening of the valve and crosses the geometrical centre of the mitral annulus. The aorto-mural diameter was measured perpendicular to the intercommissural diameter, crossing the geometrical centre of the mitral annulus and bisecting the LVOT. The annulus tridimensional perimeter was measured. The annulus was projected onto its best-fit plane (mitral annulus plane), and the projected area and perimeter were measured. The annulus height was measured as the sum of the maximum out-of-plane distance on the atrial and ventricular aspects of the valve. The right and left fibrous trigones were marked and the inter-trigone distance was measured. The mitral annulus measurements are illustrated in **Figure 1A-Figure 1C**.

The heads of the inferoseptal and superolateral papillary muscles were defined as the points closest to the mitral plane. The distance between heads was measured. For each head, the following distances were recorded: the distance to the mitral annulus centroid, the projected distance to the mitral annulus plane, and the distance to the ventricular wall. The papillary muscle measurements are illustrated in **Figure 1D**.

The left ventricle long-axis diameter was defined as the greatest distance between the mitral annulus centroid and the endocardial border. The width of the left ventricle was measured at the average level of the papillary muscle heads. It was also measured midway between the mitral annulus centroid and the left ventricle apex. The measurements are summarised in **Figure 1E**.

The left atrium long-axis diameter was defined as the distance between the atrial wall and the annulus geometrical centre in the normal direction of the mitral annulus plane. The width of the atrium was measured midway between the wall and the geometrical centre in a plane that showed the widest section through the orifice of the left atrial appendage. The left atrial appendage and pulmonary veins were excluded from the width measurements. The distance of the left atrial appendage ostium from the mitral annulus plane was measured in axial and radial directions. The axial distance measurement was performed along the mitral plane normal direction, while the radial distance was measured radially outward from the mitral annulus. The measurements are illustrated in **Figure 1F** and **Figure 1G**.

The aorto-mitral angle was defined as the angle subtended by the mitral and aortic valve annulus plane. We also measured the distance between each fibrous trigone and the aortic annulus plane – defined

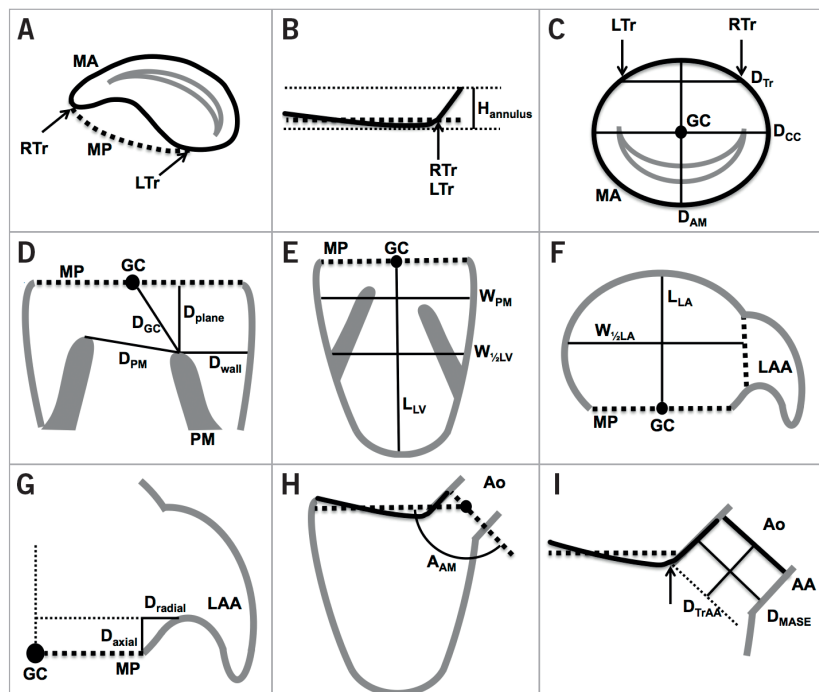


**Figure 1.** Schematic illustration of mitral valvular complex geometrical measurements. A) - C) Mitral annulus. D) Papillary muscles. E) Left ventricle. F) Left atrium. G) Left atrial appendage. H) & I) Left ventricular outflow tract. AA: aortic annulus;  $A_{AM}$ : aorto-mitral angle; Ao: aorta;  $D_{AM}$ : aorto-mural diameter;  $D_{axial}$ : axial distance to ostium of LAA;  $D_{CC}$ : intercommissural diameter;  $D_{GC}$ : papillary muscle head to GC distance;  $D_{MASE}$ : mitral annulus to septal endocardium distance;  $D_{plane}$ : papillary muscle head to mitral plane distance;  $D_{PM}$ : distance between papillary muscle heads;  $D_{radial}$ : radial distance to ostium of LAA;  $D_{Tr}$ : inter-trigone distance;  $D_{TrAA}$ : trigone to aortic annulus distance;  $D_{wall}$ : wall to papillary muscle head distance; GC: geometrical centre of mitral annulus;  $H_{annulus}$ : height of mitral annulus; LAA: left atrial appendage;  $L_{LA}$ : left atrium long-axis diameter;  $L_{LV}$ : left ventricle length; LTr: left trigone; MA: mitral annulus; MP: mitral annulus plane; RTr: right trigone;  $W_{1/2LA}$ : width of left atrium at half  $L_{LA}$ ;  $W_{1/2LV}$ : width of left ventricle at half  $L_{LV}$ ;  $W_{PM}$ : left ventricle width at level of papillary muscle heads

as the plane uniting the nadirs of each aortic leaflet. The distance between the mitral annulus and the septal endocardium was also recorded. **Figure 1H** and **Figure 1I** illustrate these measurements.

### TRANSCATHETER MITRAL VALVE DEVICE LANDING ZONE

Transcatheter mitral valve replacement devices will probably extend into the regions of the ventricular and atrial cavities immediately adjacent to the mitral annulus. To characterise this zone, splines were drawn to outline the endocardial border at 5 mm intervals on the atrial and ventricular aspects of the mitral annulus. A total of eight regions of interest were drawn at 5, 10, 15, and 20 mm above and below the mitral annulus. The area, perimeter, aorto-mural and intercommissural diameters of these regions were recorded.

### META-ANALYSIS OF STUDIES REPORTING MEASUREMENTS IN PATIENTS WITHOUT MITRAL REGURGITATION

A meta-analysis of previously published studies reporting measurements in patients without MR was performed to enable comparison of mitral valvular complex geometrical measurements between patients with and without FMR. This was necessary since the subject population from the PTOLEMY-2 trial did not include patients without MR. Studies performed in adults using computed tomography, echocardiography, and magnetic resonance imaging, as well as *post mortem* anatomical studies were screened for inclusion by a single observer. The criteria for inclusion were as follows: reporting of measurements equivalent to those performed in the current study and reporting of measurements without normalisation.

### STATISTICAL ANALYSIS

The statistical analysis was performed using MATLAB Release 2013a (MathWorks, Natick, MA, USA). Every measurement from

each subject was averaged between two independent observers. For geometrical measurements in diastole and systole, the mean and the standard deviation, as well as the median, first quartile, and third quartile were calculated. A paired-samples analysis was conducted to study dynamic variations between systole and diastole in 17 patients for whom images were available in both of these cardiac phases. Confidence intervals were computed using the bias corrected and accelerated percentile bootstrap method with 2,000 samples. For the meta-analysis of studies in patients without MR, the measurements were combined using the standard methodology<sup>7</sup>.

## Results

The baseline characteristics of the 32 patients are presented in **Table 1**. The average age was 70.1 years old, 40.6% of patients were female, and most patients suffered from left ventricular systolic dysfunction with an ejection fraction of 34.8%. Equal numbers of patients with moderate and severe FMR were included in the study.

### MITRAL VALVULAR COMPLEX GEOMETRY MITRAL ANNULUS

The mitral annulus was nearly circular with the intercommissural diameter being less than 3 mm larger than the aorto-mural diameter (diastole: 41.5 mm intercommissural vs. 40.0 mm aorto-mural; systole: 41.5 mm intercommissural vs. 38.7 mm aorto-mural) (**Table 2**). For all annulus measurements, the standard deviation was generally well above 10%, which demonstrated a relatively large amount of inter-patient variability. The annulus contracted slightly during systole (**Figure 2**). The dynamic changes of the annulus during the cardiac cycle were of relatively low amplitude – less than 2% – and were greater along the aorto-mural direction. Small statistically

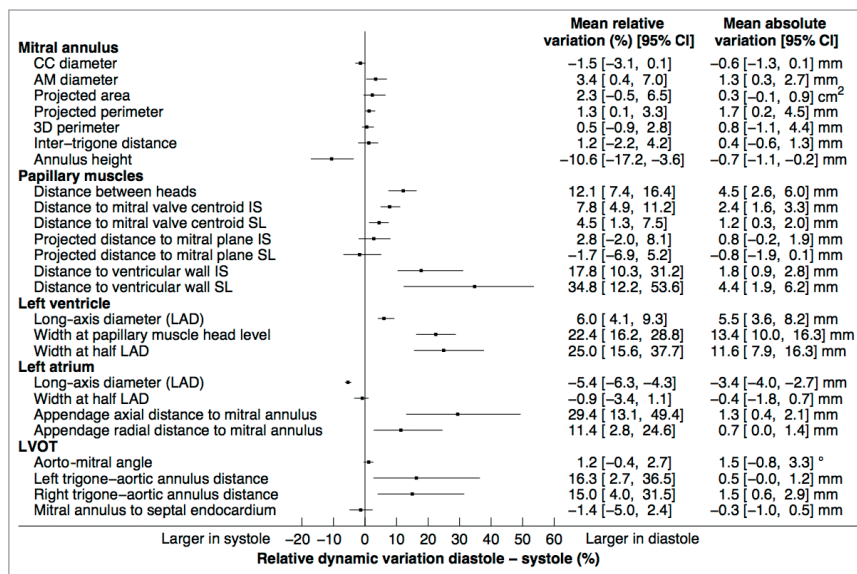


**Figure 2.** Paired-sample analysis of cardiac cycle dynamic variations in the mitral valvular complex geometrical measurements. 3D: tridimensional; AM: aorto-mural; CC: intercommissural; IA: inferoanterior; LAD: long-axis diameter; 95% CI: 95% confidence interval; SP: superoposterior

**Table 2. Mitral valvular complex geometrical measurements in all patients.**

|                                                 | Diastole (n=32) |        |                | Systole (n=17) |        |                |
|-------------------------------------------------|-----------------|--------|----------------|----------------|--------|----------------|
|                                                 | Mean±SD         | Median | [Q1, Q3]       | Mean±SD        | Median | [Q1, Q3]       |
| <b>Annulus</b>                                  |                 |        |                |                |        |                |
| CC diameter, mm                                 | 41.5±4.4        | 42.0   | [39.3, 44.0]   | 41.5±5.2       | 42.0   | [39.8, 46.5]   |
| AM diameter, mm                                 | 40.0±4.7        | 39.8   | [36.9, 43.2]   | 38.7±5.9       | 38.1   | [33.7, 45.1]   |
| Projected area, cm <sup>2</sup>                 | 13.5±2.8        | 13.7   | [11.6, 15.2]   | 13.0±3.3       | 13.0   | [10.5, 16.1]   |
| Projected perimeter, mm                         | 130.7±14.2      | 132.3  | [122.1, 139.0] | 128.1±16.3     | 128.1  | [117.2, 141.3] |
| 3D perimeter, mm                                | 135.5±14.6      | 137.3  | [127.0, 144.7] | 133.5±16.6     | 133.4  | [122.3, 146.6] |
| Inter-trigone distance, mm                      | 30.9±3.9        | 30.9   | [28.4, 33.5]   | 29.1±3.4       | 28.9   | [26.6, 30.6]   |
| Annulus height, mm                              | 6.9±1.4         | 7.3    | [5.7, 8.0]     | 7.4±1.4        | 7.6    | [6.3, 8.4]     |
| <b>Papillary muscles</b>                        |                 |        |                |                |        |                |
| Distance between heads, mm                      | 40.0±5.3        | 40.8   | [37.0, 43.3]   | 35.2±5.0       | 36.4   | [31.3, 40.3]   |
| Distance to mitral valve centroid IS, mm        | 32.9±5.4        | 32.5   | [30.4, 36.8]   | 29.7±5.4       | 29.9   | [25.2, 34.4]   |
| Distance to mitral valve centroid SL, mm        | 28.6±5.3        | 29.6   | [24.7, 32.2]   | 27.1±5.7       | 28.2   | [23.1, 31.9]   |
| Projected distance to mitral plane IS, mm       | 23.7±5.7        | 24.3   | [19.8, 27.2]   | 22.5±5.0       | 21.1   | [18.5, 27.1]   |
| Projected distance to mitral plane SL, mm       | 20.2±4.9        | 20.9   | [16.6, 24.6]   | 20.6±6.7       | 20.1   | [16.0, 25.3]   |
| Distance to ventricular wall IS, mm             | 14.9±4.6        | 15.4   | [12.9, 17.2]   | 12.8±5.2       | 13.1   | [9.1, 15.1]    |
| Distance to ventricular wall SL, mm             | 16.6±5.8        | 16.4   | [12.9, 19.5]   | 11.2±5.8       | 10.2   | [8.3, 13.9]    |
| <b>Left ventricle</b>                           |                 |        |                |                |        |                |
| Long-axis diameter (LAD), mm                    | 98.8±10.4       | 99.3   | [91.4, 105.9]  | 92.8±12.3      | 94.3   | [82.0, 101.9]  |
| Width at papillary muscle head level, mm        | 71.8±10.4       | 72.3   | [62.4, 78.9]   | 56.4±13.2      | 60.4   | [46.7, 65.1]   |
| Width at half LAD, mm                           | 65.1±11.6       | 65.5   | [56.4, 71.0]   | 51.1±19.1      | 54.0   | [32.9, 66.3]   |
| <b>Left atrium</b>                              |                 |        |                |                |        |                |
| Long-axis diameter (LAD), mm                    | 59.0±8.8        | 60.5   | [53.1, 64.3]   | 62.6±10.9      | 63.3   | [58.1, 67.2]   |
| Width at half LAD, mm                           | 57.2±8.5        | 56.5   | [51.1, 62.5]   | 57.0±9.1       | 56.1   | [49.9, 61.2]   |
| Appendage axial distance to mitral annulus, mm  | 6.6±2.6         | 6.5    | [4.5, 8.7]     | 5.2±2.5        | 5.1    | [3.4, 6.5]     |
| Appendage radial distance to mitral annulus, mm | 8.3±2.5         | 8.5    | [6.3, 9.7]     | 7.7±2.7        | 8.2    | [5.8, 9.9]     |
| <b>LVOT</b>                                     |                 |        |                |                |        |                |
| Aorto-mitral angle, degrees                     | 131.7±9.4       | 132.1  | [124.7, 137.0] | 129.7±10.5     | 130.6  | [123.8, 136.4] |
| Left trigone-aortic annulus distance, mm        | 4.8±1.7         | 4.5    | [3.8, 6.1]     | 4.6±2.3        | 4.1    | [3.1, 5.8]     |
| Right trigone-aortic annulus distance, mm       | 10.9±2.5        | 10.9   | [9.2, 12.5]    | 9.1±2.8        | 8.3    | [7.1, 11.6]    |
| Mitral annulus to septal endocardium, mm        | 21.1±3.0        | 21.4   | [19.6, 22.6]   | 20.9±3.5       | 20.3   | [17.0, 23.9]   |

AM: aorto-mural; CC: intercommissural; IS: inferoseptal; LAD: long-axis diameter; SL: superolateral

significant dynamic variations were observed for the aorto-mural diameter, the projected perimeter, and the annulus height.

#### PAPILLARY MUSCLES

The papillary muscle heads were on average more than 20 mm below the mitral annulus plane and more than 27 mm from the mitral annulus centroid (Table 2). There was, however, substantial inter-subject variability in these measurements, with standard deviations of 5 to 6 mm. The projected distance between the papillary muscle head and the mitral plane varied by less than 1.2 mm (4.5%) between systole and diastole, which was not statistically significant.

#### LEFT VENTRICLE

The width of the left ventricle was on average greater at the level of the papillary muscle heads than midway between the mitral annulus geometrical centre and the apex (Table 2).

#### LEFT ATRIUM

The left atrial width was nearly equal to the long-axis diameter (Table 2). The atrial contraction manifested itself during diastole by a 5% reduction in the long-axis diameter and a mostly constant width (Figure 2). The ostium of the left atrial appendage was further from the mitral annulus during diastole than during systole in both the radial and axial directions.

#### LVOT

Several LVOT measurements are noteworthy. The aorto-mitral angle was approximately 131° on average but varied considerably between patients with a standard variation of approximately 10° (Table 2). The angle varied slightly but not significantly during systole (Figure 2). The right trigone was approximately twice as far as the left trigone from the aortic valve annulus plane (10.9 mm vs. 4.8 mm in diastole and 9.1 mm vs. 4.6 mm in

systole). The trigone to aortic annulus distances were significantly greater during diastole (Figure 2).

### TRANSCATHETER MITRAL VALVE DEVICE LANDING ZONE GEOMETRY

The perivalvular landing zones of transcatheter prostheses were evaluated up to 20 mm away from the mitral annulus plane on its atrial and ventricular aspects (Figure 3). The aorto-mural diameter, intercommissural diameter, perimeter and surface area are smaller in systole than in diastole in the left ventricle. In the left atrium, these measurements are larger in diastole. Overall, the majority of measurements on the atrial aspect of the valve do not demonstrate a significant dynamic variation between systole and diastole (Figure 3). This also holds true for the measurements of the mitral annulus, presented at distance 0 mm.

### META-ANALYSIS OF STUDIES REPORTING MEASUREMENTS IN PATIENTS WITHOUT MITRAL REGURGITATION

From a total of 238 studies screened, 24 studies fulfilled the inclusion criteria<sup>8-31</sup>. The results are presented in Table 3 and are divided

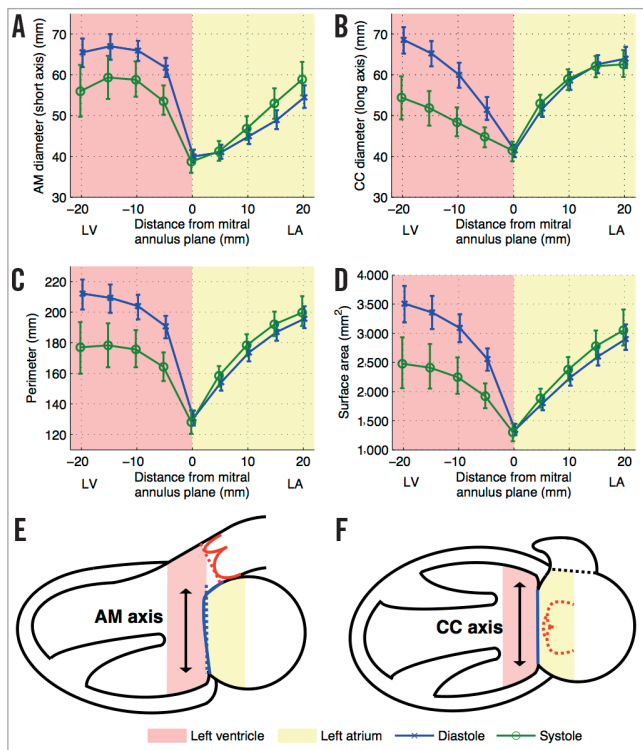


**Figure 3.** Transcatheter mitral valve device landing zone dynamic geometrical measurements. Each plot (A-D) shows a different measurement of the regions of interest drawn at the endocardial border in double-oblique planes parallel to the mitral annulus plane. The measurements at distance 0 mm represent the mitral annulus projected measurements. The error bars indicate 95% confidence intervals. A) Aorto-mural (AM) diameter. B) Intercommissural (CC) diameter. C) Perimeter. D) Surface area. E) & F) Schematic representation of the ventricular and atrial cavities. LA: left atrium; LV: left ventricle

by imaging modality in Table 4. Of the 25 measurements of the mitral valvular complex described in the current study, 11 measurements had previously been published for patients without MR. We classified measurements into systole or diastole if the cardiac phase was specified.

### Discussion

#### MITRAL VALVULAR COMPLEX GEOMETRICAL CHANGES IN FMR

FMR occurs as a result of left ventricular dysfunction following an ischaemic or non-ischaemic injury to cardiac myocytes. In affected patients, a series of changes occurs in the dimensions and dynamics of the mitral valvular complex<sup>4</sup>, most of which are reflected in the measurements presented in this study.

The mitral annulus increases in size (Figure 2, Table 2, Table 4) and systolic contraction is reduced, which agrees with previous studies<sup>11,13,17-19,24,29,32,33</sup>. The annulus also becomes more circular in patients with MR and its height is slightly reduced. This deformation is believed to contribute to the pathophysiology of FMR<sup>11,33</sup>.

Papillary muscles become misaligned in FMR. We found a large increase in the distance between papillary muscles, which is attributable to the pathological changes in the left ventricular cavity. The misalignment increases the tethering force brought to bear on the mitral valve leaflets. The resulting leaflet tenting has been shown to be a major pathophysiologic mechanism in FMR<sup>24,30</sup>. We observed that the left ventricular cavity dilates and assumes a more spherical shape in FMR, which is consistent with previous studies<sup>11,14,25,26</sup>. These changes are considered to be a strong predictor of the severity of FMR. We demonstrated a large increase in the size of the left atrium in FMR. This change is consistent with previously published literature<sup>12,14,20</sup>.

The aorto-mitral angle showed only a small, non-significant dynamic change in FMR patients, while this angle varied considerably more in patients without MR<sup>27</sup>. The systolic angle was mostly preserved but the diastolic angle was less in FMR.

#### IMPLICATIONS FOR TRANSCATHETER MITRAL VALVE DESIGN AND PATIENT SELECTION

This study is the first to evaluate the mitral valvular complex focusing on measurements relevant for transcatheter mitral valve replacement in patients with FMR. Most proposed devices are mounted on a catheter, inserted across the mitral valve and then deployed. The mitral annular dimensions are critical for the design of prostheses. We demonstrated that, in patients with FMR, the mitral annulus is approximately symmetrical between its two major axes. The annulus also contracts less than 2% in systole. This may alleviate concerns that contractions of the mitral annulus may cause excessive stress on the prosthetic valve frame. Nonetheless, we showed that the region of the left ventricle immediately below the mitral annulus is highly dynamic, which may potentially cause substantial stress on a device. Conversely, a rigid ventricular device may be prone to injure the endocardial surface of the cavity.

The frame of transcatheter valve implants may protrude on either aspect of the mitral annulus. In the ventricular cavity,

**Table 3. Meta-analysis of 24 studies reporting mitral valvular complex measurements in patients without mitral regurgitation.**

|                                 | Diastole   |     | Systole    |     | Unspecified phase |     |
|---------------------------------|------------|-----|------------|-----|-------------------|-----|
|                                 | Mean±SD    | n   | Mean±SD    | n   | Mean±SD           | n   |
| <b>Annulus</b>                  |            |     |            |     |                   |     |
| CC diameter, mm                 | 36.2±4.5   | 51  | 33.6±5.1   | 51  | 37.3±4.9          | 120 |
| AM diameter, mm                 | 31.6±7.9   | 51  | 28.8±8.0   | 51  | 28.8±3.9          | 120 |
| Projected area, cm <sup>2</sup> | 8.3±2.3    | 151 | 6.8±2.2    | 151 | 7.9±1.9           | 137 |
| Perimeter, mm                   | 107.9±16.7 | 40  | 98.2±31.5  | 40  | 96.2±11.2         | 50  |
| Inter-trigone distance, mm      | 21.0±1.0   | 5   | 23.0±2.0   | 5   | 21.7±3.7          | 43  |
| Height, mm                      | 6.5±1.6    | 73  | 8.6±2.0    | 73  | 7.0±2.1           | 53  |
| <b>Papillary muscles</b>        |            |     |            |     |                   |     |
| Distance between heads, mm      | 24.8±0.4   | 11  | 18.6±9.8   | 11  | 25.7±6.3          | 71  |
| Left ventricle                  |            |     |            |     |                   |     |
| Long-axis diameter, mm          | 88.2±8.1   | 51  | 68.2±8.6   | 51  | –                 | –   |
| Width, mm                       | 50.0±4.6   | 134 | 32.7±4.8   | 134 | –                 | –   |
| <b>Left atrium</b>              |            |     |            |     |                   |     |
| Width at half LAD, mm           | –          | –   | 36.2±4.0   | 32  | 39.4±5.3          | 72  |
| <b>LVOT</b>                     |            |     |            |     |                   |     |
| Aorto-mitral angle, degrees     | 136.2±12.6 | 24  | 129.4±11.0 | 24  | 127.6±13.5        | 38  |

AM: aorto-mitral; CC: intercommissural; LAD: long-axis diameter; n: number of subjects included in the combined measurement; SD: standard deviation

papillary muscles can represent an obstacle to the deployment of transcatheter devices. We demonstrated here that the projected distance between the mitral plane and the heads of papillary muscles – in other words, the axial obstacle-free zone for the prosthesis deployment – is approximately constant during the cardiac cycle.

Prosthetic structures extend radially outward to anchor the device within its landing zone and to prevent perivalvular leaks. We described the space available for the deployment of such anchoring structures up to 20 mm above and below the mitral annulus plane. We showed that the atrium is considerably less

**Table 4. Meta-analysis of 24 studies reporting mitral valvular complex measurements in patients without mitral regurgitation for different imaging modalities or post-mortem examination.**

|                                 | Echocardiography |     |            |     |                   |    | MRI      |    |          |    |                   |    | CT                |    | Post-mortem |    |
|---------------------------------|------------------|-----|------------|-----|-------------------|----|----------|----|----------|----|-------------------|----|-------------------|----|-------------|----|
|                                 | Diastole         |     | Systole    |     | Unspecified phase |    | Diastole |    | Systole  |    | Unspecified phase |    | Unspecified phase |    | –           |    |
|                                 | Mean±SD          | n   | Mean±SD    | n   | Mean±SD           | n  | Mean±SD  | n  | Mean±SD  | n  | Mean±SD           | n  | Mean±SD           | n  | Mean±SD     | n  |
| <b>Annulus</b>                  |                  |     |            |     |                   |    |          |    |          |    |                   |    |                   |    |             |    |
| CC diameter, mm                 | 37.1±4.3         | 40  | 34.2±5.5   | 40  | 36.6±5.3          | 78 | 33.0±3.6 | 11 | 31.2±2.5 | 11 | 39.0±4.0          | 23 | 38.0±3.0          | 19 | –           | –  |
| AM diameter, mm                 | 31.0±8.7         | 40  | 27.9±8.7   | 40  | 27.8±3.6          | 78 | 33.6±3.4 | 11 | 32.0±3.6 | 11 | 30.0±4.0          | 23 | 31.0±4.0          | 19 | –           | –  |
| Projected area, cm <sup>2</sup> | 8.2±2.3          | 140 | 6.7±2.3    | 140 | 7.5±1.8           | 66 | 8.8±1.7  | 11 | 7.9±1.3  | 11 | 8.7±1.8           | 32 | 9.4±1.4           | 19 | 6.1±1.3     | 20 |
| Perimeter, mm                   | 107.9±16.7       | 40  | 98.2±31.5  | 40  | 101.7±9.2         | 30 | –        | –  | –        | –  | –                 | –  | –                 | –  | 88.0±8.7    | 20 |
| Inter-trigone distance, mm      | 21.0±1.0         | 5   | 23.0±2.0   | 5   | –                 | –  | –        | –  | –        | –  | 24.0±3.0          | 23 | –                 | –  | 19.0±2.4    | 20 |
| Height, mm                      | 6.5±1.6          | 73  | 8.6±2.0    | 73  | 7.8±2.1           | 30 | –        | –  | –        | –  | 6.0±1.8           | 23 | –                 | –  | –           | –  |
| <b>Papillary muscles</b>        |                  |     |            |     |                   |    |          |    |          |    |                   |    |                   |    |             |    |
| Distance between heads, mm      | –                | –   | –          | –   | 23.2±3.9          | 51 | 24.8±0.4 | 11 | 18.6±9.8 | 11 | –                 | –  | –                 | –  | 32.0±7.0    | 20 |
| <b>Left ventricle</b>           |                  |     |            |     |                   |    |          |    |          |    |                   |    |                   |    |             |    |
| Long-axis diameter, mm          | –                | –   | –          | –   | –                 | –  | 88.2±8.1 | 51 | 68.2±8.6 | 51 | –                 | –  | –                 | –  | –           | –  |
| Width, mm                       | 50.7±4.8         | 83  | 33.1±5.2   | 83  | –                 | –  | 49.0±4.0 | 51 | 32.0±4.0 | 51 | –                 | –  | –                 | –  | –           | –  |
| <b>Left atrium</b>              |                  |     |            |     |                   |    |          |    |          |    |                   |    |                   |    |             |    |
| Width at half LAD, mm           | –                | –   | 36.2±4.0   | 32  | 40.3±5.2          | 53 | –        | –  | –        | –  | –                 | –  | 37.0±5.0          | 19 | –           | –  |
| <b>LVOT</b>                     |                  |     |            |     |                   |    |          |    |          |    |                   |    |                   |    |             |    |
| Aorto-mitral angle, degrees     | 136.2±12.6       | 24  | 129.4±11.0 | 24  | 127.6±13.5        | 38 | –        | –  | –        | –  | –                 | –  | –                 | –  | –           | –  |

AM: aorto-mitral; CC: intercommissural; LAD: long-axis diameter; n: number of subjects included in the combined measurement; SD: standard deviation

dynamic than the ventricle and may thus constitute a more adequate region for hosting a transcatheter device.

On the ventricular aspect, the left ventricular outflow tract is in close proximity to the mitral annulus. Thus, there exists a potential for outflow tract obstruction in some circumstances (**Figure 4**): 1) an excessively acute angle between the mitral plane and the aortic annulus, 2) small mitral annulus to septal endocardium distance, 3) excessive protrusion of the device in the left ventricular cavity, or 4) excessive flaring of the device at the ventricular end. Furthermore,

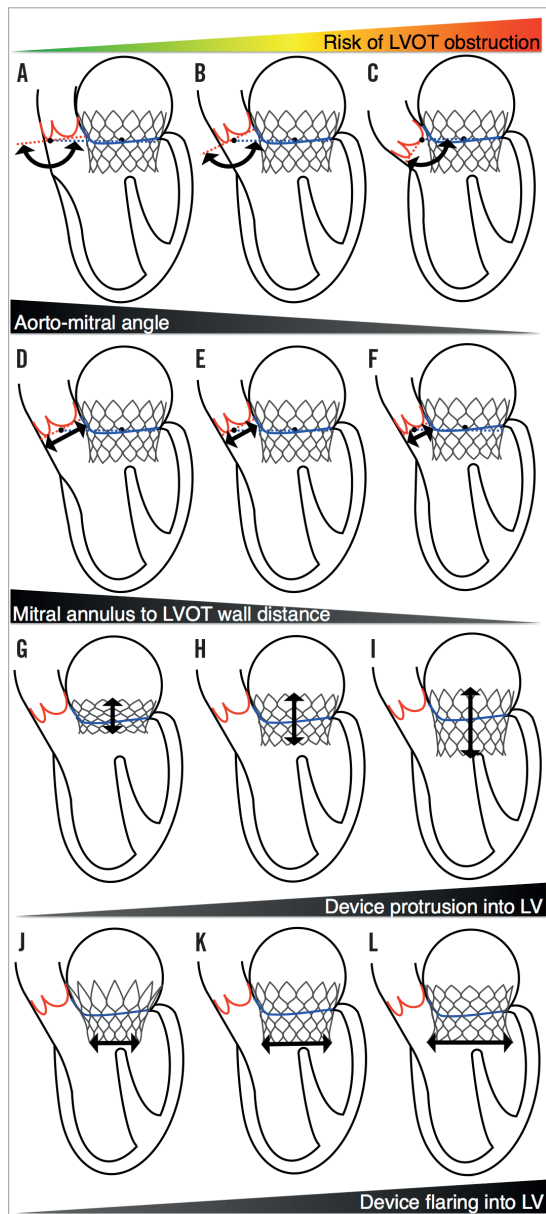


**Figure 4.** Potential mechanisms of left ventricular outflow tract obstruction in transcatheter mitral valve replacement. A-C) Increasingly acute angle between the mitral plane and the aortic annulus. D-F) Decreasing mitral annulus to septal endocardium distance. G-I) Increasing protrusion of the device in the left ventricular cavity. J-L) Increasing flaring of the device in the left ventricle. LV: left ventricle; LVOT: left ventricular outflow tract

an implant may directly impinge on the aortic valve; prosthetic valves may have anchoring structures that protrude along the LVOT and directly abut against the aortic valve leaflets. A reduced trigone to aortic annulus distance – demonstrating the proximity of the aortic valve along the LVOT – may pose an increased risk of impingement. Finally, the aorto-mitral curtain that separates the aortic valve from the left atrium is a thin and relatively compliant structure. Thus, a device deployed within the left atrium may cause a deformation of the aorto-mitral curtain and interfere with the geometry of the aortic root. Hypothetically, a direct impingement on the aortic valve may result in aortic regurgitation.

## LIMITATIONS

The scans were obtained from 15 different institutions, each of which used different CT scanner models. This variability made the systematic selection of an end-systolic and end-diastolic phase impossible. The temporal resolution of MSCT scans is also limited. The results may thus underestimate the dynamics of the structures studied. Also, the number of patients included in the study was limited.

## Conclusion

The mitral annulus is on average larger in size, more circular, and less dynamic in patients with FMR versus those without MR. The obstacle-free zone below the mitral annulus is relatively constant during the cardiac cycle. The aorto-mitral angle, which may predict the risk of left ventricular outflow tract obstruction after transcatheter device implantation, varies considerably among patients.

## Impact on daily practice

Transcatheter mitral valve replacement is a developing treatment modality for inoperable patients with severe symptomatic mitral regurgitation. This article provides a reference range for the size of cardiac structures in the patient population targeted by these interventions.

## Conflict of interest statement

P. Thériault-Lauzier is a consultant for HighLife Medical. G. Martucci is a proctor for Medtronic. R. Lange is a consultant for Medtronic. N. Piazza is a proctor and consultant for Medtronic. The other authors have no conflicts of interest to declare.

## References

1. Iung B, Vahanian A. Epidemiology of valvular heart disease in the adult. *Nat Rev Cardiol.* 2011;8:162-72.
2. Mylotte D, Osnabrugge RL, Windecker S, Lefevre T, de Jaegere P, Jeger R, Wenaweser P, Maisano F, Moat N, Sondergaard L, Bosmans J, Teles RC, Martucci G, Manoharan G, Garcia E, Van Mieghem NM, Kappetein AP, Serruys PW, Lange R, Piazza N. Transcatheter aortic valve replacement in Europe: adoption trends and factors influencing device utilization. *J Am Coll Cardiol.* 2013;62:210-9.

3. Van Mieghem NM, Piazza N, Anderson RH, Tzikas A, Nieman K, De Laet LE, McGhie JS, Geleijnse ML, Feldman T, Serruys PW, de Jaegere PP. Anatomy of the mitral valvular complex and its implications for transcatheter interventions for mitral regurgitation. *J Am Coll Cardiol.* 2010;56:617-26.
4. Sabbah HN, Rosman H, Kono T, Alam M, Khaja F, Goldstein S. On the mechanism of functional mitral regurgitation. *Am J Cardiol.* 1993;72:1074-6.
5. Thériault-Lauzier P, Mylotte D, Dorfmeister M, Andalib A, Mamane S, Chetrit M, Cecere R, Buithieu J, Martucci G, Tchetché D, Modine T, Van Mieghem N, Lange R, Windecker S, Piazza N. Quantitative multi-slice computed tomography assessment of the mitral valvular complex for transcatheter mitral valve interventions part 1: systematic measurement methodology and inter-observer variability. *EuroIntervention.* 2016;12:1011-20.
6. de Vaan J, Verstraeten L, de Jaegere P, Schultz C. The 3mensionio Valves multimodality workstation. *EuroIntervention.* 2012;7:1464-9.
7. Higgins JPT, Green S (editors). *Cochrane Handbook for Systematic Reviews of Interventions*, Version 5.1.0 [updated March 2011]; Higgins JPT, Deeks JJ (editors) Chapter 7: Selecting studies and collecting data. The Cochrane Collaboration; 2011.
8. Ahmad RM, Gillinov AM, McCarthy PM, Blackstone EH, Apperson-Hansen C, Qin JX, Agler D, Shiota T, Cosgrove DM. Annular geometry and motion in human ischemic mitral regurgitation: novel assessment with three-dimensional echocardiography and computer reconstruction. *Ann Thorac Surg.* 2004;78:2063-8.
9. Caiani EG, Fusini L, Veronesi F, Tamborini G, Maffessanti F, Gripari P, Corsi C, Naliato M, Zanobini M, Alamanni F, Pepi M. Quantification of mitral annulus dynamic morphology in patients with mitral valve prolapse undergoing repair and annuloplasty during a 6-month follow-up. *Eur J Echocardiogr.* 2011;12:375-83.
10. Chandra S, Salgo IS, Sugeng L, Weinert L, Tsang W, Takeuchi M, Spencer KT, O'Connor A, Cardinale M, Settlemier S, Mor-Avi V, Lang RM. Characterization of degenerative mitral valve disease using morphologic analysis of real-time three-dimensional echocardiographic images: objective insight into complexity and planning of mitral valve repair. *Circ Cardiovasc Imaging.* 2011;4:24-32.
11. D'Ancona G, Biondo D, Mamone G, Marrone G, Pirone F, Santise G, Sciacca S, Pilato M. Ischemic mitral valve regurgitation in patients with depressed ventricular function: cardiac geometrical and myocardial perfusion evaluation with magnetic resonance imaging. *Eur J Cardiothorac Surg.* 2008;34:964-8.
12. Kim DH, Handschumacher MD, Levine RA, Choi YS, Kim YJ, Yun SC, Song JM, Kang DH, Song JK. In vivo measurement of mitral leaflet surface area and subvalvular geometry in patients with asymmetrical septal hypertrophy: insights into the mechanism of outflow tract obstruction. *Circulation.* 2010;122:1298-307.
13. De Simone R, Wolf I, Mottl-Link S, Hoda R, Mikhail B, Sack FU, Meinzer HP, Hagl S. A clinical study of annular geometry and dynamics in patients with ischemic mitral regurgitation: new insights into asymmetrical ring annuloplasty. *Eur J Cardiothorac Surg.* 2006;29:355-61.
14. Gertz ZM, Raina A, Saghy L, Zado ES, Callans DJ, Marchlinski FE, Keane MG, Silvestry FE. Evidence of atrial functional mitral regurgitation due to atrial fibrillation: reversal with arrhythmia control. *J Am Coll Cardiol.* 2011;58:1474-81.
15. Grewal J, Suri R, Mankad S, Tanaka A, Mahoney DW, Schaff HV, Miller FA, Enriquez-Sarano M. Mitral annular dynamics in myxomatous valve disease: new insights with real-time 3-dimensional echocardiography. *Circulation.* 2010;121:1423-31.
16. Hueb AC, Jatene FB, Moreira LF, Pomerantzef PM, Kallas E, de Oliveira SA. Ventricular remodeling and mitral valve modifications in dilated cardiomyopathy: new insights from anatomic study. *J Thorac Cardiovasc Surg.* 2002;124:1216-24.
17. Kaji S, Nasu M, Yamamuro A, Tanabe K, Nagai K, Tani T, Tamita K, Shiratori K, Kinoshita M, Senda M, Okada Y, Morioka S. Annular geometry in patients with chronic ischemic mitral regurgitation: three-dimensional magnetic resonance imaging study. *Circulation.* 2005;112:1409-14.
18. Kaplan SR, Bashein G, Sheehan FH, Legget ME, Munt B, Li XN, Sivarajan M, Bolson EL, Zeppa M, Arch MZ, Martin RW. Three-dimensional echocardiographic assessment of annular shape changes in the normal and regurgitant mitral valve. *Am Heart J.* 2000;139:378-87.
19. Kihara T, Gillinov AM, Takasaki K, Fukuda S, Song JM, Shiota M, Shiota T. Mitral regurgitation associated with mitral annular dilation in patients with lone atrial fibrillation: an echocardiographic study. *Echocardiography.* 2009;26:885-9.
20. Killeen RP, Arnous S, Martos R, Abbara S, Quinn M, Dodd JD. Chronic mitral regurgitation detected on cardiac MDCT: differentiation between functional and valvular aetiologies. *Eur Radiol.* 2010;20:1886-95.
21. Kwan J, Shiota T, Agler DA, Popovic ZB, Qin JX, Gillinov MA, Stewart WJ, Cosgrove DM, McCarthy PM, Thomas JD. Real-time three-dimensional echocardiography study. Geometric differences of the mitral apparatus between ischemic and dilated cardiomyopathy with significant mitral regurgitation: real-time three-dimensional echocardiography study. *Circulation.* 2003;107:1135-40.
22. Maffessanti F, Marsan NA, Tamborini G, Sugeng L, Caiani EG, Gripari P, Alamanni F, Jeevanandam V, Lang RM, Pepi M. Quantitative analysis of mitral valve apparatus in mitral valve prolapse before and after annuloplasty: a three-dimensional intraoperative transesophageal study. *J Am Soc Echocardiogr.* 2011;24:405-13.
23. Ormiston JA, Shah PM, Tei C, Wong M. Size and motion of the mitral valve annulus in man. I. A two-dimensional echocardiographic method and findings in normal subjects. *Circulation.* 1981;64:113-20.
24. Otsuji Y, Kumanohoso T, Yoshifuku S, Matsukida K, Koriyama C, Kisanuki A, Minagoe S, Levine RA, Tei C. Isolated annular dilation does not usually cause important functional mitral regurgitation: comparison between patients with lone atrial

fibrillation and those with idiopathic or ischemic cardiomyopathy. *J Am Coll Cardiol*. 2002;39:1651-6.

25. Schiros CG, Dell'Italia LJ, Gladden JD, Clark D 3rd, Aban I, Gupta H, Lloyd SG, McGiffin DC, Perry G, Denney TS Jr, Ahmed MI. Magnetic resonance imaging with 3-dimensional analysis of left ventricular remodeling in isolated mitral regurgitation: implications beyond dimensions. *Circulation*. 2012;125:2334-42.

26. Suri RM, Grewal J, Mankad S, Enriquez-Sarano M, Miller FA Jr, Schaff HV. Is the anterior intertrigonal distance increased in patients with mitral regurgitation due to leaflet prolapse? *Ann Thorac Surg*. 2009;88:1202-8.

27. Veronesi F, Corsi C, Sugeng L, Mor-Avi V, Caiani EG, Weinert L, Lamberti C, Lang RM. A study of functional anatomy of aortic-mitral valve coupling using 3D matrix transesophageal echocardiography. *Circ Cardiovasc Imaging*. 2009;2:24-31.

28. Veronesi F, Caiani EG, Sugeng L, Fusini L, Tamborini G, Alamanni F, Pepi M, Lang RM. Effect of mitral valve repair on mitral-aortic coupling: a real-time three-dimensional transesophageal echocardiography study. *J Am Soc Echocardiogr*. 2012;25:524-31.

29. Watanabe N, Ogasawara Y, Yamaura Y, Wada N, Kawamoto T, Toyota E, Akasaka T, Yoshida K. Mitral annulus flattens in ischemic mitral regurgitation: geometric differences between inferior and

anterior myocardial infarction: a real-time 3-dimensional echocardiographic study. *Circulation*. 2005;112:1458-62.

30. Yiu SF, Enriquez-Sarano M, Tribouilloy C, Seward JB, Tajik AJ. Determinants of the degree of functional mitral regurgitation in patients with systolic left ventricular dysfunction: A quantitative clinical study. *Circulation*. 2000;102:1400-6.

31. Yu HY, Su MY, Liao TY, Peng HH, Lin FY, Tseng WY. Functional mitral regurgitation in chronic ischemic coronary artery disease: analysis of geometric alterations of mitral apparatus with magnetic resonance imaging. *J Thorac Cardiovasc Surg*. 2004;128:543-51.

32. Mihalatos DG, Joseph S, Gopal A, Bercow N, Toole R, Passick M, Grimson R, Norales A, Reichek N. Mitral annular remodeling with varying degrees and mechanisms of chronic mitral regurgitation. *J Am Soc Echocardiogr*. 2007;20:397-404.

33. Kumanohoso T, Otsuji Y, Yoshifuku S, Matsukida K, Koriyama C, Kisanuki A, Minagoe S, Levine RA, Tei C. Mechanism of higher incidence of ischemic mitral regurgitation in patients with inferior myocardial infarction: quantitative analysis of left ventricular and mitral valve geometry in 103 patients with prior myocardial infarction. *J Thorac Cardiovasc Surg*. 2003;125:135-43.